Catalysis Science & Technology

Accepted Manuscript

ROYAL SOCIETY OF CHEMISTRY

www.rsc.org/catalysis

Catalysis Science & Technology

ARTICLE

One-pot synthesis of Pt catalysts based on layered double hydroxides: an application in propane dehydrogenation

Received 00th January 20xx,
Accepted 00th January 20xx

DOI: 10.1039/x0xx00000x

www.rsc.org/

M. Filez,[a] E. A. Redekop,[a] H. Poelman,[a] V. V. Galvita,[a] M. Meledina,[b] S. Turner,[b] G. Van Tendeloo,[b] C. Detavernier[c] and G. B. Marin[a]

Simple methods for producing noble metal catalysts with well-defined active sites and improved performance are highly desired in chemical industry. However, the development of such methods still presents a formidable synthetic challenge. Here, we demonstrate a one-pot synthesis route for the controlled production of bimetallic Pt-In catalysts based on the single-step formation of Mg,Al,Pt,In-containing layered double hydroxides (LDHs). Besides their simple synthesis, these Pt-In catalysts exhibit superior propane dehydrogenation activity compared to their multi-step synthesized analogs. The presented material serves as a showcase for the one-pot synthesis of a broader class of LDH-derived mono- and multimetallic Pt catalysts. The compositional flexibility provided by LDH-materials can pave the way towards high-performing Pt-based catalysts with tunable physicochemical properties.

Introduction

Heterogeneous catalysts are the key enablers of multifarious chemical reactions, making them essential in the vast majority of industrial chemical processes.[1-2] Amongst them, mono- and bimetallic Pt-based catalysts constitute a class of utmost importance, as they promote reactions ranging from alkane (de)hydrogenation to oxygenate reforming and NO_x/CO exhaust gas removal.[3] Besides their wide applicability, they function as quintessential model catalysts which have been intensely researched for decades. Nowadays, it is widely established that the size and composition of bimetallic Pt nanoparticles strongly impact the overall catalyst performance.[2, 4] For this reason, high precision synthesis techniques have been developed for the fabrication of tailored Pt-based nanoparticles.[5-10] However, such techniques are typically very expensive and complex, as they involve multiple synthesis steps, and lack scalability for producing industrially relevant quantities. More simple synthesis procedures – such as wet chemical impregnation – can offer suitable alternatives, but generally lack proper control over the metal nanoparticle size and composition. As a consequence, a pressing need has arisen for simple, cheap and scalable catalyst synthesis methods which allow for rational design of nanostructured catalysts with fine control over the active sites.

Layered double hydroxides (LDHs) have emerged as versatile and high-performing materials applicable in diverse fields, including catalysis, photochemistry and pharmaceutics.[11-14] This large family of materials consists of cationic 2D brucite-type $[M_{1-a}^{2+}M_a^{3+}(OH)_2]^{a+}$ layers, containing octahedrally OH-coordinated di- and trivalent metal cations.[15-16] By electrostatic interaction with charge-compensating anions and water, these 2D layers self-assemble into a stacked configuration of alternating cationic brucite-type layers and anionic interlayer galleries, yielding $[M_{1-a}^{2+}M_a^{3+}(OH)_2]^{a+}[A_{a/n}]^{n-}.mH_2O$ LDHs. These LDH materials have proven efficient as catalysts, catalyst precursors and catalyst supports. Their high compositional flexibility – by tuning the type of metal cations and/or interlayer anions – enables the formation of nanoarchitectures with adaptable physicochemical properties. In addition, the uniform distribution of metal cations in the brucite-type layers yields controllable and well-dispersed (bimetallic) nanoparticles after calcination and reduction treatment. For example, some studies report on one-pot synthesized LDH-derived nanocatalysts, including supported bimetallic Cu-Zn or Pd-Ga nanoparticles, exhibiting superior performance during reaction, such as methanol synthesis and acetylene hydrogenation respectively.[17-20] Some attempts have been made to synthesize LDH-derived monometallic Pt catalysts in multiple steps.[21-23] However, to the best of our knowledge, single-step synthesis of Pt-containing LDHs as precursors for tailored (multi)metallic Pt-based catalysts has not been reported to date.

Here, we demonstrate a one-pot synthesis protocol for the production of Mg,Al,Pt,In-LDHs based on the single-batch intercalation of Pt^{4+} species in the interlayer galleries of precipitated $[(Mg)_{1-a}^{2+}(Al/In)_a^{3+}(OH)_2]^{a+}$ layers. After

[a] Laboratory for Chemical Technology (LCT), Ghent University, Technologiepark 914, B-9052 Ghent, Belgium.
[b] Electron Microscopy for Materials Science (EMAT), University of Antwerp, Groenenborgerlaan 171, B-2020 Antwerp, Belgium.
[c] Conformal Coating of Nanomaterials (CoCooN), Ghent University, Krijgslaan 281/S1, B-9000 Ghent, Belgium.

Electronic Supplementary Information (ESI) available: Performance of Pt/Mg(Pt)(Al)O_x monometallic and Pt-Ga/Mg(Ga)(Al)O_x bimetallic catalysts. See DOI: 10.1039/x0xx00000x

consecutive calcination and reduction, these LDHs yield well-dispersed Pt-In nanoparticles on Mg(Pt)(In)(Al)O_x supports with superior performance during propane dehydrogenation. Indeed, the addition of a promotor element to Pt, such as In[24], Sn[25], Ga[26], Ge[27], Cu[28], Zn[29], strongly increases the alkene selectivity and prevents rapid catalyst deactivation by coke formation. The presented material serves as a showcase for the cheap and scalable one-step synthesis of a broader family of Pt-containing LDHs and LDH-derived catalysts. Throughout Mg,Al,Pt,In-LDH synthesis and activation, X-ray absorption spectroscopy (XAS) and X-ray diffraction (XRD) are used to probe the short and long range structural characteristics, respectively. High-angle annular dark field scanning transmission electron microscopy (HAADF-STEM) combined with spatially resolved energy-dispersive X-ray spectroscopy (EDX) is used complementary to XAS and XRD to provide spatial resolution. This work exemplifies the intelligent design of multifunctional Pt-based catalysts based on one-pot synthesized LDH precursors.

Experimental

First, an aqueous solution (250 mL) of $Mg(NO_3)_2.6H_2O$ (29 g, Sigma-Aldrich, 98 – 102%), $Al(NO_3)_3.9H_2O$ (4.2 g, Sigma-Aldrich, 98.5%) and $In(NO_3)_3.xH_2O$ (0.07 g, Sigma-Aldrich, 99.99%) was mixed with an aqueous solution (250 mL) of Na_2CO_3 (0.6 g, EMD Chemicals Inc., 99.5%), NaOH (6 g, Fisher Scientific, 98.3%) and H_2PtCl_6 (0.05 g, Company), and was kept at pH ~ 14. After 24h of aging at room temperature, the precipitate was filtered, washed with deionized water until pH 7 was reached and dried at 110 °C, yielding the 'Mg,Al,Pt,In-LDH' sample. Subsequent calcination and H_2 reduction treatment – both for 4 hours at 650 °C – resulted in 'Mg(Pt)(In)(Al)O_x' and 'Pt-In/Mg(Pt)(In)(Al)O_x' samples, respectively.

ICP-AES. Inductively coupled plasma atomic emission spectrometry (ICP-AES) (IRIS Advantage system, Thermo Jarrell Ash) was used to obtain the chemical composition of the synthesized material. To obtain the concentrations, Mg(Pt)(In)(Al)O_x was mineralized by peroxide fusion. Mg(Pt)(In)(Al)O_x contains 0.45 wt% Pt, 1.64 wt% In, 43.4 wt% Mg, and 5.8 wt% Al.

XAS. *Ex situ* XAS measurements were performed at the SuperXAS beamline of the SLS synchrotron (2.4 GeV, 400 mA, PSI, Villigen – Switzerland). In addition, *in situ* XAS measurements were executed at the DUBBLE beam line[30-31] of the ESRF synchrotron (6 GeV, current 160 – 200 mA, Grenoble - France). At DUBBLE, 2 mm quartz capillaries were connected to gas lines by swagelok® fittings and subsequently mounted below the gas blower (FMB Oxford). The DUBBLE gas rig system was employed to regulate the gas flows through the capillary.[30-31] All XAS measurements were recorded in transmission mode at the Pt L_{III} edge. XAS data analysis was executed by using the Demeter 0.9.13 software package.[32-33] Background subtraction and normalization were performed for extracting the XANES and EXAFS signals.

XRD. Crystallographic phase analysis of the materials was conducted by using a Siemens Diffractometer Kristalloflex D5000, with Cu Kα radiation (λ = 0.154 nm). The patterns were collected in a 2θ range from 5° to 90° with a step of 0.02° and 30 s counting time at each angle.

HAADF-STEM imaging and EDX mapping. HAADF-STEM imaging and EDX elemental mapping were carried out on a FEI Titan "cubed" microscope equipped with and aberration corrector and large solid angle "Super-X" EDX detector and operated at 120 kV. The convergence semi-angle used for STEM was 21 mrad, the acceptance inner semi-angle for HAADF-STEM imaging was 85 mrad.

Results and discussion

During one-pot synthesis of Mg,Al,Pt,In-LDH, an aqueous solution of $Mg(NO_3)_2.6H_2O$, $Al(NO_3)_3.9H_2O$ and $In(NO_3)_3.xH_2O$ is mixed with an aqueous solution of NaOH, Na_2CO_3 and H_2PtCl_6 (see Experimental Section). The initial NaOH-Na_2CO_3-H_2PtCl_6 solution is yellow-colored, which is characteristic of basic H_2PtCl_6-containing aqueous solutions.[34] Upon mixing the two

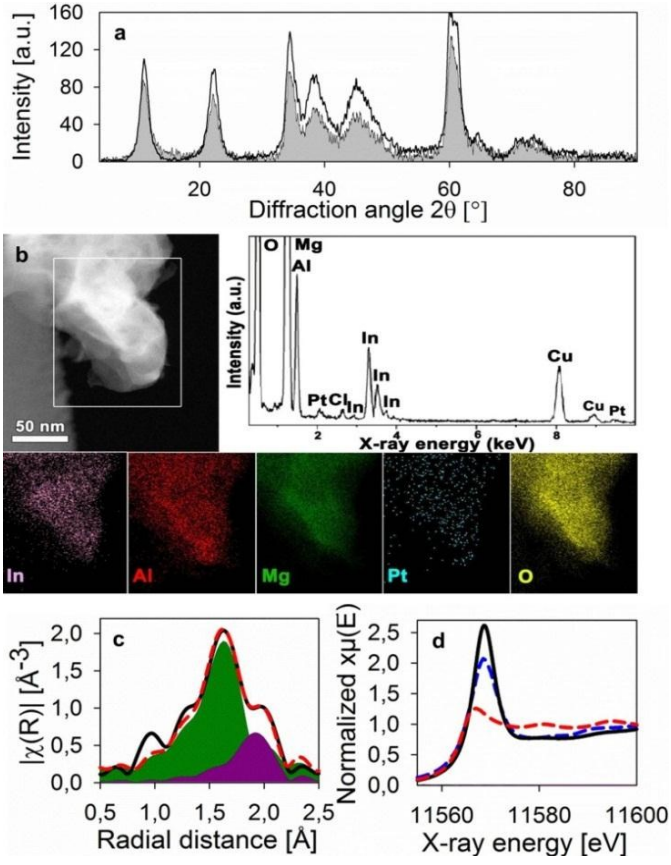

Figure 1. Presented data are measured on 'Mg,Al,Pt,In-LDH', i.e. the sediment obtained after co-precipitation of Mg-Al-In- and Pt-containing aqueous solutions. (a) XRD profile of Mg,Al,Pt,In-LDH (grey area) and a Mg,Al-LDH reference (solid black line); (b) HAADF-STEM overview image of a precipitate grain and the corresponding EDX chemical maps of the region marked by the white rectangle in the overview image. The EDX spectrum summed over the full region shows that Mg, Al, Pt, Cl and In are present within the precipitate; (c) Pt L_{III} edge Mg,Al,Pt,In-LDH Fourier transformed EXAFS magnitude (black solid line), Pt-O + Pt-Cl model fit (red dashed line) between R = 1.1 – 2.2 Å (R-factor = 0.005), Pt-O (green area) and Pt-Cl (purple area) contributions; (d) Pt L_{III} edge XANES spectrum of Mg,Al,Pt,In-LDH (black solid line), bulk PtO_2 (blue dashed line) and Pt (red dashed line) references.

solutions, rapid precipitation is observed due to the self-assembly of LDHs.[15, 16] After precipitation, the solution still exhibits a yellow color which strongly indicates that Pt is not as yet incorporated inside the LDH structure at this stage. However, after a few hours of aging, the yellow-colored mixture gradually evolves to a transparent solution, suggesting that Pt is being inserted inside the pre-existing Mg,Al,In-LDH precipitate, yielding Mg,Al,Pt,In-LDH.

An XRD scan of the precipitate – measured after aging, filtering, washing and drying – indeed displays typical LDH diffraction peaks (Figure 1.a, filled area) as compared to a Mg,Al-LDH reference (Figure 1.a, solid black line). In addition, the presence of Mg, Al, Pt, Cl and In inside this LDH structure is evidenced by the EDX spectrum of a separate precipitate grain (Figure 1.b), confirming that Mg,Al,Pt,In-LDH is formed.

The local environment and electronic state of Pt inside the LDH precipitate is monitored by Pt L_{III} EXAFS (Figure 1.c) and XANES (Figure 1.d), respectively. Modeling of the Fourier transformed (FT) EXAFS peak between R ~ 1.1 and 2.2 Å only succeeds when both Pt-O and Pt-Cl shells are included (Figure 1.c). Although the Pt-O contribution is dominant (N_{Pt-O} = 4.3 ± 0.3, R_{Pt-O} = 1.99 ± 0.01 Å), the Pt-Cl peak constitutes a significant part of the FT EXAFS peak shape (N_{Pt-Cl} = 1.0 ± 0.2, R_{Pt-Cl} = 2.29 ± 0.01 Å). EXAFS modeling results therefore suggest that octahedrally coordinated Pt species reside inside the LDH structure as $[PtCl_1(OH)_5]^{-2}$-type complexes (see below). XANES is consistent with these EXAFS results as the strong white line feature, which exceeds the one of bulk PtO_2, is characteristic for Cl^--OH^- ligand exchanged Pt complexes (Figure 1.d).[35]

After mixing of the Mg,Al,In- and Pt-containing solutions, the pH in the solution is maintained at ~ 14. At this pH and Pt precursor concentration (Experimental Section), octahedrally coordinated $[PtCl_6]^{2-}$ anions undergo rapid hydrolysis reactions yielding $[PtCl_{6-x}(H_2O)_x]^{-2+x}$ species.[36] During co-precipitation of LDHs, it is known that tetravalent cations (Pt^{+4}) cannot be incorporated inside di- and trivalent (Mg^{+2}, Al^{+3}, In^{+3}) metal containing brucite-type layers.[15, 16] Moreover, the rapidly formed neutral/cationic $[PtCl_{6-x}(H_2O)_x]^{-2+x}$ species do not interact with the precipitated LDH structure – in contrast to OH^- and CO_3^{2-} anions – as they cannot act as charge-compensating agents. In addition, $[PtCl_{6-x}(H_2O)_x]^{-2+x}$ complexes are not compatible with the $(Mg_{1-a}{}^{+2}(In/Al)_a{}^{+3}(OH)_2)^{+a}$ brucite-layer structure due to the presence of Cl^- and H_2O^0 ligands – instead of OH^- – around Pt. This causes the Pt complexes to remain in the aqueous phase and results in a yellow-colored solution immediately after Mg,Al,In-LDH precipitation. Subsequent slower ligand exchange reactions between Cl^- or H_2O^0 and OH^- eventually result in the formation of $[PtCl_{6-x}(OH)_x]^{-2}$-type complexes (x > 3) at current conditions.[36] Hence, only after LDH assembly, these slowly formed anionic complexes undergo interaction with cationic $(Mg_{1-a}{}^{+2}(In/Al)_a{}^{+3}(OH)_2)^{+a}$ layers to neutralize the net charge of the LDH structure.[22] Such interaction leads to the intercalation of $[PtCl_1(OH)_5]^{-2}$ complexes (XAS, Figure 1.c) inside the interlayer galleries, and results in a color change in the mixture from yellow to transparent during aging treatment.

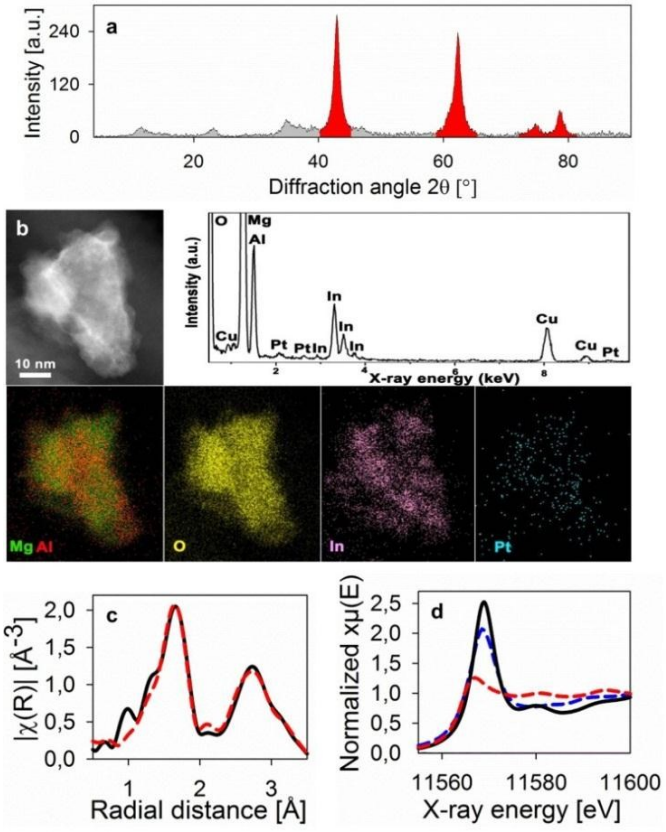

Figure 2. Presented data are measured on 'Mg(Pt)(In)(Al)O_x', i.e. obtained after calcination of initial Mg,Al,Pt,In-LDH. (a) XRD profile showing peak features (red areas) typical of periclase MgO. In addition, some remainders of the Mg,Al,Pt,In-LDH structure can be observed; (b) HAADF-STEM image of a Mg(Pt)(In)(Al)O_x grain and corresponding EDX elemental maps, showing that Mg, Al, Pt and In are present within the mixed metal oxide, together with a summed EDX spectrum from the full region; (c) Pt L_{III} edge Fourier transformed EXAFS magnitude of Mg(Pt)(In)(Al)O_x (black solid line) and MgO model fit (red dashed line) between R = 1.1 – 3.5 Å (R-factor = 0.012); (d) Pt L_{III} edge XANES spectrum of Mg(Pt)(In)(Al)O_x (black solid line), bulk PtO_2 (blue dashed line) and Pt (red dashed line) references.

After calcination of Mg,Al,Pt,In-LDH for 4 h at 650 °C, the XRD profile displays intense peak features around 44°, 62°, 74° and 79° (Figure 2.a). This is characteristic for the formation of 3D MgO-type mixed metal oxides (MMO) as a result of the collapse of the 2D lamellar LDH structure.[37, 38] The elemental EDX maps in Figure 2.b in combination with the Z-contrast HAADF-STEM image show rather heterogeneous distributions of Mg, Al and In cations throughout the inspected grain. Besides the typical MgO-type diffraction from the MMO and some traces of recovered LDH (memory effect), no significant XRD peaks are observed.[39] This suggests that in addition to the dominant MgO-type MMOs, some minor fractions of amorphous or nanocrystalline (mixed) metal oxide phases are formed during calcination.

Starting from binary Mg,Al-LDHs, Bellotto et al. pointed out that calcination eventually yields disordered spinel-type Mg(Al)O_x mixed oxides, containing octahedral Mg^{+2} and tetrahedral Al^{+3} cations.[38] After initial dehydration of the Mg,Al-LDH structure, octahedral Al^{+3} cations rearrange by migrating from the Mg,Al-hydroxide layer to tetrahedral sites in the interlayer space. Further heating to 400 °C causes

interlayer anions to decompose, and induces complete dehydroxylation of the material. This eventually leads to the formation of a 3D structure consisting of a regular oxygen cubic closed packed MgO-type network with a disordered Mg^{+2}/Al^{+3} cation distribution at the interstices. Similar to binary Mg,Al-LDHs, quaternary Mg,Al,Pt,In-LDHs are also expected to yield Mg(Pt)(In)(Al)O_x MMOs – as suggested by the MgO-type diffraction reflections in XRD – in addition to a minority of XRD-insensitive amorphous/nanocrystalline (mixed) oxides (EDX).

In order to pinpoint the precise location of Pt in the calcined material, XAS measurements are used to probe its local environment as well as its electronic state. When implementing MgO as a structural model around Pt, convergence between the FT EXAFS signal of calcined Mg,Al,Pt,In-LDH and the model is obtained (Figure 2.c). The coordination numbers of N_{Pt-O} = 5.4 ± 0.4 and N_{Pt-Mg} = 12.6 ± 4 are compatible with the 6-fold O and 12-fold Mg coordination around Mg within MgO, i.e. N_{Mg-O} = 6 and N_{Mg-Mg} = 12, respectively. In fact, the N_{Pt-Mg} coordination contains the contributions of both Mg and Al neighbors around Pt, as these two atomic species cannot be discriminated by EXAFS modeling. These EXAFS results strongly suggest that Pt is incorporated inside a Mg(Pt)(In)(Al)O_x MgO-type MMO structure. The latter finding is supported by the fact that the Pt-Mg coordination of atomically dispersed Pt atoms on MgO-type supports amounts to 4.1 ± 0.7, a significantly lower number compared to the current case.[40]

XANES (Figure 2.d) both complements and supports the EXAFS results. The Pt L_{III} white line height of Mg(Pt)(In)(Al)O_x exceeds the height of bulk PtO_2, demonstrating that 5d electron states of Pt atoms inside Mg(Pt)(In)(Al)O_x are more empty than in PtO_2.[41, 42] The mixed metal environment around Pt therefore induces more electron transfer from Pt towards Mg(Pt)(In)(Al)O_x as compared to pure PtO_2. The basic oxide properties exerted by the most abundant Mg^{2+} cations within Mg(Pt)(In)(Al)O_x are responsible for the strong interaction between Mg(Pt)(In)(Al)O_x and Pt.[43, 44] This leads to strong Pt oxidation and more empty 5d electron states, and results into the observed intense Pt L_{III} white line.

The possibility of Pt-incorporation inside the MMO structure after calcination implies that the original $[PtCl_1(OH)_5]^{-2}$ anions, unlike other interlayer anions, are relatively immobile and stable within the initial LDH structure. Before calcination, $[PtCl_1(OH)_5]^{-2}$ complexes are therefore suggested to have relatively strong bonds with the Mg(In)(Al)-OH groups of the layered $(Mg_{1-a}^{+2}(In/Al)_a^{+3}(OH)_2)^{+a}$ hydroxide surface. Upon calcination, initial dehydration of Mg,Al,Pt,In-LDH, In^{+3}/Al^{+3} migration to the interlayer galleries, and OH^- and CO_3^{-2} decomposition is followed by dehydroxylation and oxidation of the metal hydroxides (metal = Mg^{+2}, Al^{+3}, In^{3+}, Pt^{+4}). As shown by XRD, HAADF-STEM and XAS, this results in the collapse of the 2D lamellar LDH structure and leads to the formation of 3D MgO-type Mg(Pt)(In)(Al)O_x MMOs plus a minority of amorphous/ nanocrystalline (mixed) oxides.

The final step of catalyst activation for one-pot synthesized Mg,Al,Pt,In-LDHs consists of a H_2 TPR treatment on

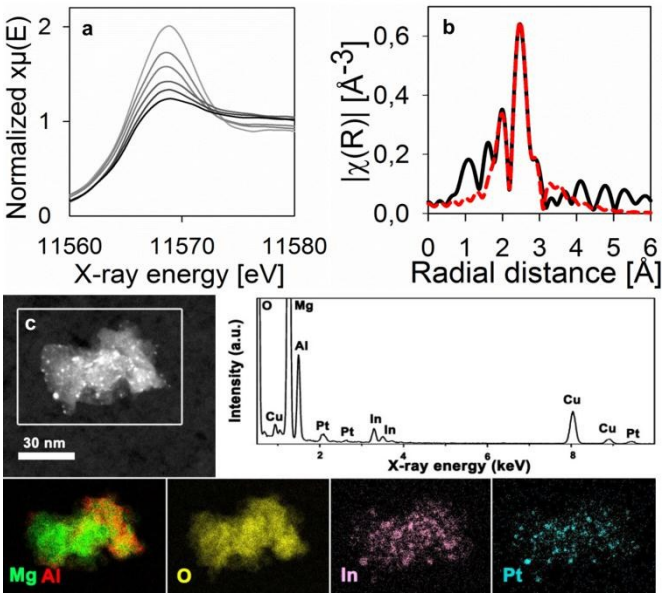

Figure 3. Presented data are measured on 'Pt-In/Mg(Pt)(In)(Al)O_x', i.e. obtained after H_2 TPR of Mg(Pt)(In)(Al)O_x. (a) Pt L_{III} edge XANES spectra recorded during H_2 TPR (from grey to black): white line decrease and edge shift to higher energies; (b) Fourier transformed EXAFS magnitude of Pt-In/Mg(Pt)(In)(Al)O_x (black solid line) and Pt-In + Pt-Pt model fit (red dashed line) between R = 1.8 – 3.1 Å (R-factor = 0.005); (c) HAADF-STEM image of a Pt-In/Mg(Pt)(In)(Al)O_x grain and corresponding EDX elemental maps. The EDX spectra show the presence of both Pt and In at the same locations.

Mg(Pt)(In)(Al)O_x to 650 °C. *In situ* XANES spectra recorded during this H_2 TPR display a gradual decrease of the Pt L_{III} edge white line, which is characteristic of Pt reduction (Figure 3.a). In addition, a significant edge shift to higher energies is observed during Pt reduction, indicating that Pt-In alloying is occurring.[40, 45] FT EXAFS modeling evidences the presence of both In and Pt neighbors around Pt, i.e. N_{Pt-In} = 4.8 ± 0.4 (R_{Pt-In} = 2.65 ± 0.01 Å) while N_{Pt-Pt} = 2.2 ± 0.5 (R_{Pt-Pt} = 2.76 ± 0.02 Å) (Figure 3.b), and therefore suggests the formation of Pt-In clusters. HAADF-STEM imaging confirms the formation of dispersed nanoparticles (bright dots) decorating the Mg(Pt)(In)(Al)O_x support surface (Figure 3.c). EDX elemental mapping shows nano-sized islands with increased Pt and In concentration, which indeed demonstrates that the clusters formed during H_2 TPR consist of Pt-In nanoparticles.

In the course of H_2 TPR, hydrogen reduces Pt cations from the Mg(Pt)(In)(Al)O_x support (XANES, Figure 3.a). This causes Pt to gain mobility owing to the scission of strong Mg-O-Pt bonds. Upon temperature increase, partially reduced Pt migrates across the support and eventually forms thermodynamically stable Pt-In nanoparticles (XAS, HAADF-STEM).[46] Three mechanisms, which could however occur simultaneously, can be responsible for Pt-In alloying. Firstly, partially reduced Pt – either as migrating atoms over the support or, in a later stage, as stabilized nanoparticles – dissociates hydrogen which spills over to the Mg(Pt)(In)(Al)O_x support.[47] Subsequent long-range transport of H to In^{3+} sites results in the partial reduction of In^{3+} into $In^{\delta+}$. These moderately mobile $In^{\delta+}$ species undergo short-range transport to Pt atoms/clusters which fully reduce $In^{\delta+}$ to In^0 upon immediate stabilization inside Pt-In nano-alloys.[47] Secondly, single atoms of Pt migrating over the

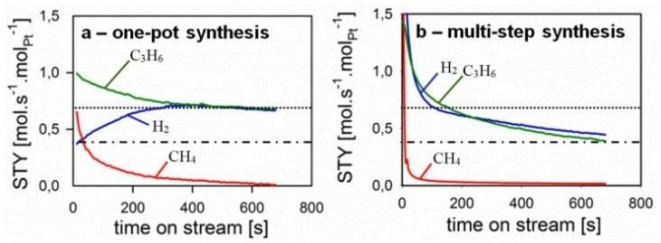

Figure 4. Catalytic propane dehydrogenation at 600 °C ($W_{cat}/F_{propane,0}$ = 4 kg_{cat}·s·mol^{-1} and $P_{propane,0}$ = 5 kPa at a total pressure of 101.3 kPa): site-time yield (STY) vs. time on stream: (a) one-pot Pt-In/Mg(Pt)(In)(Al)O_x and (b) multi-step synthesized Pt-In/Mg(In)(Al)O_x. The dotted (dash-dotted) line shows the steady state propylene STY for the one-pot (multi-step) Pt-In catalyst.

support could also directly interact with In^{3+} sites and establish immediate Pt-In alloying after full reduction of In^{3+} to In^0.[41, 46] Thirdly, at 650 °C in H_2, a fraction of the In^{3+}-phase could reduce directly to In^0, liquefy/vaporize, undergo liquid/gas phase transport to Pt and establish Pt-In alloys.[48, 49]

In Figure 4, the one-pot synthesized Pt-In/Mg(Pt)(In)(Al)O_x catalyst performance is compared to the performance of multi-step synthesized Pt-In/Mg(In)(Al)O_x, the latter obtained through wet impregnation of Pt on Mg(In)(Al)O_x (see ref 43 and 44). The plots display the transient activity flows of C_3H_6, CH_4 and H_2 as a function of time elapsed since the introduction of a C_3H_8 step into the reactor. For all catalysts, the initial transient period is dominated by non-selective side reactions other than propane dehydrogenation, including deep dehydrogenation (coke formation) and hydrogenolysis.[50, 51] CH_4 is coming from hydrogenolysis of C_2-C_3 hydrocarbons, C_2 being produced by hydrogenolysis of C_3.[26, 50, 52] C_2's are completely decomposed into methane, coke and hydrogen by hydrogenolysis and dehydrogenation which occur in parallel with other side reactions.[26, 50-52] After a few minutes, the most reactive sites are blocked by coke formation. This inhibits the occurrence of non-selective side reactions, causing the reactor outlet flow to become more rich in C_3H_6 and H_2. When comparing the stabilized steady-state activity of the two catalysts, it is clear that the one-pot synthesized Pt-In/Mg(Pt)(In)(Al)O_x exerts higher activity and similar selectivity as compared to multi-step synthesized Pt-In/Mg(In)(Al)O_x catalysts. Notably, the one-pot synthesized Pt-In/Mg(Pt)(In)-(Al)O_x catalyst also provides long-term stability (hours) during propane dehydrogenation after the initial transient period (Figure S-2), in contrast to previously reported Pt-based dehydrogenation catalysts.[53] As shown in Supporting Information, one-pot synthesized Pt/Mg(Pt)(Al)O_x catalysts also exhibit some activity. However, due to the catalyst monometallic nature, initial coking leads to the blockage of the Pt active sites in Pt/Mg(Pt)(Al)O_x, yielding low activity for propylene. This emphasizes the necessity of incorporating a promoting element in the original LDH-structure, which is demonstrated here.

Figure 4.a and Figure 4.b show that one-pot synthesized Pt-In catalysts exhibit significantly higher propane dehydrogenation activity in steady-state regime relative to their multi-step synthesized analogues. In contrast, the initial propane dehydrogenation activity is ~ 50% higher for the multi-step synthesized catalyst compared to the one-pot synthesized one. The underlying cause for these differences in catalytic behaviour can be attributed to dissimilarities in nanoparticle size distribution and composition of the studied catalysts. More precisely, during multi-step synthesis, wet impregnation of Pt on a Mg(In)(Al)O_x support results in a bi- or multimodal particle size distribution[50], in contrast to the more uniform nanoparticle size distribution obtained after one-pot synthesis (Figure 3.c). Indeed, the more intimate contact between Pt and In during one-pot synthesis results in a more homogeneous nanoparticle size distribution and alloy composition.

H_2 chemisorption experiments on the one-pot and multi-step synthesized catalysts show that the number of Pt sites per m² of catalyst is very similar for both cases (for same wt% of Pt). The discrepancy in catalytic performance between the two types of catalysts can thus be attributed to the differing nature of their active Pt sites. For the multi-step synthesized Pt-In catalysts, it can be assumed that – in general – two different types of Pt sites are present: (1) low coordinated (small clusters) and (2) highly coordinated sites (large clusters), owing to their bimodal cluster size distribution.[50] Low coordinated sites are expected to exhibit high activity initially, but deactivate rapidly on the short time-scale depicted in Figure 4.b. Highly coordinated sites are less active during propane dehydrogenation and also deactivate, as large Pt nanoparticles are gradually encapsulated by carbon deposits.[54] However, their deactivation is slower than the deactivation of low coordinated sites, which explains the residual activity in Figure 4.b. In contrast, one-pot synthesized Pt-In catalysts are more abundant in Pt sites with intermediate average coordination, owing to their narrow and monomodal size distribution. These Pt sites with intermediate coordination are moderately active during propane dehydrogenation (Figure 4.a), but are able to shift carbon deposits to the support material[25, 54] – thereby guaranteeing long-term catalyst stability. The PDH reaction mechanism itself is changing as a function of the particle size,[54-56] which can also contribute to the kinetic differences observed in Figure 4.a and Figure 4.b. Another factor that could affect this difference in catalytic performances is the compositional inhomogeneity of the nanoparticles on multi-step synthesised catalysts.[56] The initially high, but rapidly decreasing PDH activity in Figure 4.b may be related to the monometallic Pt nanoparticles that are present on the multi-step synthesised catalysts along with the bimetallic nanoparticles. The intricate role of the nature of the Pt active sites and their relative abundances therefore play an important role in the resulting macroscopic catalytic performance, as presented in Figure 4, and should be studied in more detail.

As discussed in the previous paragraphs, the propane dehydrogenation activity per exposed Pt site – the most expensive catalyst component – is higher for the one-pot synthesized Pt-In catalysts relative to its multi-step synthesized counterpart. These results show that the methodology of one-pot synthesis for the facile and scalable production of bimetallic Pt-based nanocatalysts is not only cost efficient

during catalyst synthesis, but also during dehydrogenation reaction. More specifically, the cost of catalyst production can be significantly reduced by eliminating all-but-one synthesis steps. In addition, the propylene production cost during operation also decreases as higher yields of propylene can be obtained with the same amount of catalyst. Notably, these trends of superior dehydrogenation performance are also observed for one-pot synthesized Pt-Ga catalysts (Supporting Information). This demonstrates that the proposed one-pot synthesis strategy is in fact not only applicable to Pt-In/Mg(Pt)(In)(Al)O_x catalysts, but also to a broad family of Pt-based bi- or multimetallic LDH-derived catalysts.

Conclusions

A one-pot synthesis method is established for the production of tailored bimetallic Pt-based catalysts, herein exemplified by the single-step synthesis of Mg,Al,Pt,In-LDHs. Calcination of these quaternary LDHs at 650 °C results in the collapse of their 2D lamellar structure, yielding 3D Mg(Pt)(In)(Al)O_x mixed metal oxides with a MgO-type structure. Subsequent H_2 reduction treatment triggers atomic transport of reducible Pt and In cations, eventually causing well-dispersed Pt-In alloyed nanoparticles to be formed on the Mg(Pt)(In)(Al)O_x support. The one-pot synthesized Pt-In/Mg(Pt)(In)(Al)O_x catalyst exhibits superior performance during catalytic dehydrogenation of propane as compared to multi-step synthesized Pt-In catalysts. Their simple, cheap and scalable synthesis protocol as well as their high product yield make one-pot Pt-In/Mg(Pt)(In)(Al)O_x catalysts particularly attractive for industrial use. In addition, the compositional flexibility of Pt-containing LDHs allows for the rational design of the catalyst properties and fine control over the catalyst active sites. The future exploitation of this compositional flexibility could pave the way to more efficient multimetallic Pt-based catalysts.

Acknowledgements

This work was supported by the Fund for Scientific Research Flanders (FWO: G.0209.11), the 'Long Term Structural Methusalem Funding by the Flemish Government', the IAP 7/05 Interuniversity Attraction Poles Programme – Belgian State – Belgian Science Policy, and the Fund for Scientific Research Flanders (FWO-Vlaanderen) in supplying financing of beam time at the DUBBLE beam line of the ESRF and travel costs and a post-doctoral fellowship for S.T. The authors acknowledge the assistance from the DUBBLE (XAS campaign 26-01-979) and SuperXAS staff (Proposal 20131191). E. A. Redekop acknowledges the Marie Curie International Incoming Fellowship granted by the European Commission (Grant Agreement No. 301703). The authors also express their gratitude to O. Janssens for performing *ex situ* XRD characterization.

Notes and references

1 R. Schlögl, *Angew. Chem. Int. Ed.*, 2015, **54**, 3465.
2 G. A. Somorjai, H. Frei and J. Y. Park, *J. Am. Chem. Soc.*, 2009, **131**, 16589.
3 W. Yu, M. D. Porosoff, and J. G. Chen, *Chem. Rev.*, 2012, **112**, 5780.
4 S. Shan, J. Luo, L. Yang and C.-J. Zhang, *Catal. Sci. Technol.*, 2014, **4**, 3570.
5 X. D. Wang, L. Altmann, J. Stover, V. Zielasek, M. Baumer, K. Al-Shamery, H. Borchert, J. Parisi and J. Kolny-Olesiak, *Chem. Mater.*, 2013, **25**, 1400.
6 R. Schlögl, *Angew. Chem. Int. Ed.*, 2004, **43**, 1628.
7 W. Zang, G. Li, L. Wang and X. Zhang, *Catal. Sci. Technol.*, 2015, **5**, 2532.
8 P. Lara and K. Philippot, *Catal. Sci. Technol.*, 2014, **4**, 2445.
9 T. S. Ahmadi, Z. L. Wang, T. C. Green, A. Henglein and M. A. El-Sayed, *Science*, 1996, **272**, 1924.
10 C.-K. Tsung, J. N. Kuhn, W. Huang, C. Aliaga, L.-I. Hung, G. A. Somorjai and P. Yang, *J. Am. Chem. Soc.*, 2009, **131**, 5816.
11 Q. Xiao, Z. Liu, A. Bo, S. Zavahir, S. Sarina, S. Bottle, J. D. Riches and H. Zhu, *J. Am. Chem. Soc.*, 2015, **137**, 1956.
12 X. Zou, A. Goswami and T. Asefa, *J. Am. Chem. Soc.*, 2013, **135**, 17242.
13 M. A. Thyveetil, P. V. Coveney, H. C. Greenwell and J. L. Suter, *J. Am. Chem. Soc.*, 2008, **130**, 4742.
14 K. Teramura, S. Iguchi, Y. Mizuno, T. Shishido and T. Tanaka, *Angew. Chem. Int. Ed.***,** 2012, **51**, 8008.
15 G. Fan, F. Li, D. G. Evans and X. Duan, *Chem. Soc. Rev.*, 2014, **43**, 7040.
16 S. He, Z. An, M. Wei, D. G. Evans and X. Duan, *Chem. Comm.*, 2013, **49**, 5912.
17 M. Behrens, I. Kasatkin, S. Kühl and G. Weinberg, *Chem. Mater.*, 2010, **22**, 386.
18 S. Kühl, A. Tarasov, S. Zander, I. Kasatkin and M. Behrens, *Chem. – Eur. J.*, 2014, **20**, 3782.
19 A. Ota, J. Kröhnert, G. Weinberg, I. Kasatkin, E. L. Kunkes, D. Ferri, F. Girgsdies, N. Hamilton, M. Armbrüster, R. Schlögl and M. Behrens, *ACS Catal.*, 2014, **4**, 2048.
20 M. Behrens, *Catal. Tod.*, 2015, *246*, 46.
21 J. H. Lee, H. Kim, Y. S. Lee and D.-Y. Jung, *ChemCatChem*, 2014, **6**, 113.
22 O. B. Belskaya, T. I. Gulyaeva, N. N. Leont'eva, V. I. Zaikovskii, T. V. Larina, T. V. Kireeva, V. P. Doronin and V. A. Likholobov, *Kinet. Catal.*, 2011, **52**, 876.
23 O. B. Belskaya, T. I. Gulyaeva, V. P. Talsi, M. O. Kazakov, A. I. Nizovskii, A. V. Kalinkin, V. I. Bukhtiyarov and V. A. Likholobov, *Kinet. Catal.*, 2014, **55**, 786.
24 J. Wu, Z. Peng, A. T. Bell, *Appl. Catal. A*, 2014, **470**, 208.
25 J. Wu, Z. Peng, A. T. Bell, *J. Catal.*, 2014, **311**, 161.
26 G. Siddiqi, P. Sun, V. Galvita, A. T. Bell, *J. Catal.*, 2010, **274**, 200.
27 A. D. Ballarini, S. R. de Miguel, A. A. Castro, Scelza, O. A., *Appl. Catal. A*, 2013, **467**, 235.
28 Z. Han, S. Li, F. Jiang, T. Wang, X. Ma, J. Gong, *Nanoscale*, 2014, **6**, 10000.
29 J. Silvestre-Albero, M. A. Sanchez-Castillo, R. He, A. Sepulveda-Escribano, F. Rodriguez-Reinoso, J. A. Dumesic, *Catal. Lett.*, 2001, **74**, 17.
30 S. Nikitenko, A. M. Beale, A. M. J. van der Eerden, S. D. M. Jacques, O. Leynaud, M. G. O'Brien, D. Detollenaere, R. Kaptein, B. M. Weckhuysen and W. Bras, *Synchrotron Rad.*, 2008, **15**, 632.
31 V. Martis, A. M. Beale, D. Detollenaere, D. Banerjee, M. Moroni, F. Gosselin and W. Bras, *J. Synchrotron Rad.*, 2014, **21**, 462.
32 J. J. Rehr, J. M. Deleon, S. I. Zabinsky and R. C. Albers, *J. Am. Chem. Soc.,* 1991, **113**, 5135.

33 B. Ravel and M. Newville, *J. Synchrot. Radiat.,* 2005, **12**, 537.
34 S. Chen, Y. Wu, S. Tao, P. Cui, W. Chu, X. Chen and Z. Wu, *J. Mol. Struct.,* 2013, **1041**, 39.
35 X. Chen, W. Chu, L. Wang and Z. Wu, *J. Mol. Struct.,* 2009, **920**, 40.
36 W. A. Spieker, J. Liu, J. T. Miller, A. J. Kropf and J. R. Regalbuto, *Appl. Catal. A-Gen.,* 2002, **232**, 219.
37 M. Bellotto, B. Rebours, O. Clause, J. Lynch, D. Bazin and E. Elkaïm, *J. Phys. Chem.,* 1996, **100**, 8527.
38 M. Bellotto, B. Rebours, O. Clause, J. Lynch, D. Bazin and E. Elkaïm, *J. Phys. Chem.,* 1996, **100**, 8535.
39 V. Rives, *Mater. Chem. Phys.,* 2002, **75**, 19.
40 M. Filez, E. A. Redekop, H. Poelman, V. V. Galvita and G. B. Marin, *Anal. Chem.,* 2015, **87**, 3520.
41 M. Filez, H. Poelman, R. K. Ramachandran, J. Dendooven, K. Devloo-Casier, E. Fonda, C. Detavernier and G. B. Marin, *Catal. Today,* 2014, **229**, 2.
42 M. Huebner, D. Koziej, M. Bauer, N. Barsan, K. Kvashnina, M. D. Rossell, U. Weimar and J. D. Grunwaldt, *Angew. Chem. Int. Ed.,* 2011, **50**, 2841.
43 Y. Nagai, K. Dohmae, Y. Ikeda, N. Takagi, T. Tanabe, N. Hara, G. Guilera, S. Pascarelli, M. A. Newton, O. Kuno, H. Jiang, H. Shinjoh and S. Matsumoto, *Angew. Chem. Int. Ed.,* 2008, **47**, 9303.
44 Y. Nagai, T. Hirabayashi, K. Dohmae, N. Takagi, T. Minami, H. Shinjoh and S. Matsumoto, *J. Catal.,* 2006, **242**, 103.
45 P. Sun, G. Siddiqi, W. C. Vining, M. Chi and A. T. Bell, *J. Catal.,* 2011, **282**, 165.
46 M. Filez, E. A. Redekop, H. Poelman, V. V. Galvita, R. K. Ramachandran, J. Dendooven, C. Detavernier and G. B. Marin, *Chem. Mater.,* 2014, **26**, 5936.
47 M. Filez, E. A. Redekop, H. Poelman, V. V. Galvita, M. Meledina, S. Turner, G. Van Tendeloo, A. T. Bell and G. B. Marin, *ACS Catal.,* (submitted).
48 H. Okamoto, *J. Phase Equilib. Diffus.*, 2005, **26**, 399.
49 T. Bielz, H. Lorenz, W. Jochum, R. Kaindl, F. Klauser, B. Klötzer, S. Penner, *J. Phys. Chem. C,* 2010, **114**, 9022.
50 E. A. Redekop, V. V. Galvita, H. Poelman, V. Bliznuk, C. Detavernier and G. B. Marin, *ACS Catal.* 2014, **4**, 1812.
51 J. J. H. B. Sattler, J. Ruiz-Martinez, E. Santillan-Jimenez and B. M. Weckhuysen, *Chem. Rev.,* 2014, **114**, 10613.
52 V. Galvita, G. Siddiqi, P. Sun, A. T. Bell, *J. Catal.*, 2010, **271**, 209.
53 Z. Nawaz, F. Baksh, J. Zhu, F. Wei, *J. Ind. Eng. Chem.*, 2013, **19**, 540.
54 Z. Peng, F. Somodi, S. Helveg, C. Kisielowski, P. Specht; A. T. Bell, *J. Catal.*, 2012, **286**, 22.
55 J. Zhu, M.-L. Yang, Y. Yu, Y.-A. Zhu, Z.-J. Sui, X.-G. Zhou, A. Holmen, D. Chen, *ACS Catal.*, 2015, **5**, 6310.
56 L. Bednarova, C. E. Lyman, E. Rytter, A. Holmen, *J. Catal.*, 2002, **211**, 335.

One-pot synthesis of Mg,Al,Pt,In-layered double hydroxides (LDHs) yields well-dispersed Pt-In NPs after O_2 and H_2 activation. These nanocatalysts display increased propane dehydrogenation activity and exemplify the potential for deriving a broad class of multimetallic Pt catalysts from LDHs.